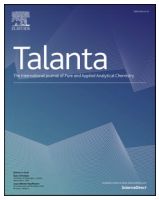
Talanta 270 (2024) 125497



Contents lists available at ScienceDirect

Talanta

journal homepage: www.elsevier.com/locate/talanta





A "signal off-on" fluorescence bioassay based on 2D-MoS_2-tetrahedral DNA bioconjugate for rapid virus detection

Daniel García- Fernández [a], Laura Gutiérrez- Gálvez [a], Manuel Vázquez Sulleiro [b], Marina Garrido [b], David López-Diego [c], Mónica Luna [c], Emilio M. Pérez [b], Tania García-Mendiola [a,d,**], Encarnación Lorenzo [a,b,d,*]

[a] Departamento de Química Analítica y Análisis Instrumental, Universidad Autónoma de Madrid, 28049, Madrid, Spain
[b] IMDEA-Nanociencia, Ciudad Universitaria de Cantoblanco, 28049, Madrid, Spain
[c] Instituto de Micro y Nanotecnología IMN-CNM, CSIC (CEI UAM+CSIC), 28760, Tres Cantos, Madrid, Spain
[d] Institute for Advanced Research in Chemical Sciences (IAdChem), Universidad Autónoma de Madrid, 28049, Madrid, Spain

ARTICLE INFO

Handling Editor: Prof A Campiglia

Keywords:
Nanostructured bioconjugate
Molybdenum disulphide
Tetrahedral DNA nanostructures
Fluorescence
SARS-CoV-2

ABSTRACT

In this work we present the preparation of a 2D molybdenum disulphide nanosheets (2D-MoS_2) and tetrahedral DNA nanostructures (TDNs) bioconjugate, and its application to the development of a bioassay for rapid and easy virus detection. The bioconjugate has been prepared by using TDNs carrying the capture probe labelled with 6-carboxyfluoresceine (6-FAM). As case of study to assess the utility of the assay developed, we have chosen the SARS-CoV-2 virus. Hence, as probe we have used a DNA sequence complementary to a region of the SARS-CoV-2 ORF1ab gene (TDN-ORF-FAM). This 6-FAM labelled capture probe is located on the top vertex of the tetrahedral DNA nanostructure, the three left vertices of TDNs have a thiol group. These TDNs are bounded to 2D-MoS_2 surface through the three thiol groups, allowing the capture probe to be oriented to favour the biorecognition reaction with the analyte. This biorecognition resulting platform has finally been challenged to the detection of the SARS-CoV-2 ORF1ab gene sequence as the target model by measuring fluorescence before and after the hybridization event with a detection limit of 19.7fM. Furthermore, due to high sensitivity of the proposed methodology, it has been applied to directly detect the virus in nasopharyngeal samples of infected patients without the need of any amplification step. The developed bioassay has a wide range of applicability since it can be applied to the detection of any pathogen by changing the probe corresponding to the target sequence. Thus, a novel, hands-on strategy for rapid pathogen detection has proposed and has a high potential application value in the early diagnosis of infections causes by virus or bacteria.

1. Introduction

Nanobioconjugates are hybrid components that combine the properties of nanomaterials and biomolecules. They show improved properties than the individual materials due to the synergistic effect. Among biomolecules, bioconjugation includes lipids, antibodies, nucleic acids or other biologically active molecules. These molecules can be paired with different substances that may introduce interesting properties (dyes, ligands, drugs, fluorophores, etc.) [1]. During the last years, bioconjugates have experienced a recent advance, allowing deeper approaches into different fields. Currently, bioconjugates are mostly used in medical chemistry, particularly dedicated to therapy, drug delivery or imaging [2–4], however, there are some fields like DNA sensing which have not been completely approached and developed [5,6].

In terms of sensing, bioconjugates have been mostly applied to the development of biosensors for the detection of different biomarkers or pathogens, such as dengue virus (DENV-2), lung cancer P53 protein or thrombin [7–9]. However, during the recent years, there has been a new trend aimed towards the use of bioconjugates to detect analytes right away [10,11] bringing out several advantages, such as greater simplicity, ease of use and less cost.

The detection of specific DNA sequences is a promising approach for the selective detection of pathogens since the diseases caused by these organisms constitute one of the most dangerous threats to public health

* Corresponding author. Departamento de Química Analítica y Análisis Instrumental, Universidad Autónoma de Madrid, 28049, Madrid, Spain.
** Corresponding author. Institute for Advanced Research in Chemical Sciences (IAdChem), Universidad Autónoma de Madrid, 28049, Madrid, Spain.
E-mail addresses: tania.garcia@uam.es (T. García-Mendiola), encarnacion.lorenzo@uam.es (E. Lorenzo).

https://doi.org/10.1016/j.talanta.2023.125497
Received 27 July 2023; Received in revised form 22 November 2023; Accepted 25 November 2023
Available online 15 December 2023
0039-9140/© 2023 The Authors. Published by Elsevier B.V. This is an open access article under the CC BY-NC-ND license (http://creativecommons.org/licenses/by-nc-nd/4.0/).

due to their usual high mortality rate. During the last two decades, three outbreaks of human coronaviruses have been reported, including SARS-CoV-2 (2019), so early detection of this type of infection is essential to stop the spread of the disease. Since traditional techniques struggle to detect pathogens in an early stage of the infection, there is great interest in developing highly rapid, simple, affordable and sensitive virus detection techniques [12]. DNA optical assays, fluorescent assays i.e., can meet these properties and provide a promising alternative due to its advantages including ease of use, low cost and robustness.

Although numerous detection platforms that use DNA as recognition element have been described in the literature [13], there are not many methods based on the use of bioconjugates between nanomaterials and DNA despite the many advantages that these can provide, in particular, the development of rapid and selective detection methods [14].

Among nanomaterials, two-dimensional nanomaterials due to their unique properties, such as large specific area, active surface interaction with biomolecules and facile surface functionalization, provide advantages in developing novel detection technologies with fast response and high sensitivity [15]. Single- and few-layered transition metal dichalcogenide nanosheets (TMD-NS), in particular molybdenum disulphide (2D-MoS_2), has proved many promising applications in the fields of sensors and electronics due to its exceptional optical, electronic and electrochemical properties [16]. As well, this nanomaterial is capable of immobilize thiolated DNA probes given that organic molecules with thiol group tend to repair or eliminate sulphur vacancies of the MoS_2 lattice, resulting in the molecular functionalization of the substrate [17]. Taking all this into consideration, 2D-MoS_2 proves to be a nanomaterial, not very explored yet, but with great potential for bioconjugate preparation with synergic properties, allowing better performance than the individuals.

Besides that, the use of DNA as an emerging material for nanoscale engineering is a great deal of interest due to its characteristics including flexibility, specificity and programmability. These features allow the use of DNA probes with the objective of building nanostructures based on probe self-assembly. DNA self-assembly hinges on the pairing of nitrogenous bases, thus, oligonucleotides are used as "building materials" ignoring their genetical information. One of the methods is the so-called DNA Origami [18] based on the use of a long single-strand viral DNA (known as scaffold) that folds into the desired structure using short DNA viral fragments (known as staples). This method requires a complex design and preparation; thus, new alternatives have been developed, specifically, the synthesis of three-dimensional polyhedral DNA nanostructures. These nanostructures are built through base complementarity of short DNA single strands and have captured the attention of the scientific community [19]. Among them, tetrahedral DNA nanostructure have been emerging and gradually used in the biosensing field [20,21]. DNA tetrahedrons functionalized with capture probes can be developed and provide considerable advantages for enhancing biomolecular recognition on bioassay platforms [22]. These advantages are achieved due to the specific orientation, well defined spacing between probes and high stability of these tetrahedral DNA nanostructures. Although the use of TDNs have been reported previously, it is a deal of great interest since it provides advantages concerning the recognition event through hybridization in DNA biosensor development and by end in the performance of the final device. Hence, the design of new type of these structures and its application is a subject that needs to be studied in order to bring out their full potential. Overmore, its combination with two-dimensional nanomaterials has yet to be deeply explored [23].

The major attraction of fluorophore-labelled oligonucleotide probe systems relays on the strongly enhanced fluorescence signals observed upon hybridization with target or complementary sequences of DNA [24]. However, when fluorophores are used there are two major difficulties. Firstly, the poor photostability of fluorophores due to possible photobleaching effects that may result in irreproducible signals. Secondly, the low signal amplification obtained through dye-labelled DNA probes because these probes can only be modified with one or a few fluorescent molecules, thus, fluorescent signal is too weak to detect low concentrations of analyte. Consequently, new strategies have been explored in order to achieve photostable and strong fluorescence signals [25].

Taking these goals into account, in the present work we propose, for the first time, a tetrahedral DNA nanostructures (TDNs) and molybdenum disulphide nanosheets (2D-MoS_2)-based fluorescence bioconjugate for the rapid and easy detection of SARS-CoV-2, which has been chosen as case of study due to the pandemic that continues affecting the mass population, nonetheless, the method is pliable enough to detect other virus or pathogens if needed. The developed method shows improved analytical characteristic compared to similar detection methods reported in the literature and has been directly applied to detect the virus in nasopharyngeal samples of infected patients without the need of any amplification step.

2. Materials and methods

2.1. Chemicals

Sodium phosphate dibasic dihydrate ($Na_2HPO_4{\cdot}2H_2O$), sodium phosphate monobasic monohydrate ($NaH_2PO_4{\cdot}H2O$), sodium chloride (NaCl), magnesium chloride ($MgCl_2$), tris(hydroxymethyl)aminomethane (Tris, $NH_2C(CH_2OH)_3$), hydrochloric acid (HCl) and sodium hydroxide (NaOH) were purchased from Merck.

DNA oligonucleotides (Table S1) were also purchased from Merck. The design of Tetra-A, Tetra-B, Tetra-C and Tetra-D was previously reported by (Pei et al., 2010). The red regions correspond to the capture probe and its complementary strand, while the rest of the regions with the same colour represent the complementary regions of the nanotetrahedron scaffold. For selectivity studies 2 interferents (SARS-CoV-1 and Influenza A) and one mutated (a Single Nucleotide Polymorphism (SNP) from ORF1ab) sequences were used (see Table S1 in Supporting Information).

2.2. SARS-CoV-2 nasopharyngeal samples from patients

RNA from inactivated swab nasopharyngeal samples obtained from COVID-19 patients and supplied by Hospital Ramón y Cajal (Madrid) was extracted with the QIAamp Viral RNA Qiagen kit. The total RNA obtained was eluted in water free of RNase, and its concentration was measured using a Nanodrop prior to its storage at – 80 °C. To avoid any cross-contamination between samples and/or during their manipulation by the operator, all procedures were performed in P2-biosecurity cabinets with spatial and temporal separation between COVID-19 positive and negative samples. Two positive samples with different viral load (cycle threshold values (Cts) of 15 (patient 2, P2) and 29 (patient 1, P1)) and a negative sample or non-infected patient (with a Cts value above the threshold (~35)) were analyzed by the developed method after 1:10 dilution in sterilized purified Milli-Q water and results compared with those obtained by RT-qPCR.

2.3. Apparatus

For fluorescent measurements, a Varian Cary Eclipse spectrofluorometer and quartz cuvettes with a 1.0 cm optical path were used.

UV–visible spectra were recorded from 200 to 800 nm in 1.0 cm quartz cells in a double-beam PharmaSpec UV-1700 series spectrophotometer from Shimadzu Corporation.

TDN synthesis was carried out using a MiniAmpPlusTM Thermal Cycler.

Purified water Millipore Milli-Q-System (18.2 MΩ cm) was used for the preparation of all solutions. All materials and solutions were sterilized in a Nüve OT012 autoclave before being used.

Raman spectra of different stages in the biosensor preparation were recorded on a Bruker Senterra confocal Raman microscope (Bruker

Optic, Ettlingen, Germany) by using the following parameters: objective 100X; laser excitation: 532 nm, 2 mW; resolution: 3–5 cm-1; integration time: 10 s; coadditions: 10; slit opening: 50 × 1000 μm.

For the nanostructured bioconjugate preparation a Hettich Zentrifugen Universal 320 R centrifuge and 3 KDa Centrifugal Filter Units purchased from Merck were used.

Atomic force microscopy (AFM) images were obtained with a Nanotec Electrónica AFM system (provided by Nanotec Electrónica, Madrid, Spain), using silicon cantilevers (PPP-FM Nanosensors, 2.8 N/m nominal spring constant and a resonant frequency of 75 kHz in air), in dynamic mode. The acquisition and processing of images were carried out with WSxM 5.0 Develop 9.4. software [27].

An incident light fluorescence microscope Axioskop 2MAT (purchased from ZEISS, Oberkochen, Germany) (AxioVs40AC v. 4.1 software) with a mercury short arc lamp HBO 50 W/AC L1 (OSRAM) was used for acquiring the fluorescence microscopy images.

SEM images were acquired with a FEI instrument (VERIOS 460), with xT microscope Control v. 5.5.2 software, provided by FEI, Netherlands.

2.4. Procedures

2.4.1. Liquid phase exfoliation of 2D-MoS_2

In a round-flask of 250 mL volume, 150 mg of bulk MoS_2 was dispersed in 150 mL of 2-propanol and water (7:3 vol mixture) (Giovanelli, Castellanos-Gomez, and Pérez 2017). The mixture was cooled down at 2.5 °C in a Minichiller Hubber and sonicated during an hour using an ultrasonic probe (Vibracell 75115, Bioblock Scientific, 500 W) with an amplitude of 40%. After sonication, the black suspension was transferred to six 50 mL conical centrifuge tubes and centrifugated in an Allegra X-15R Beckman Coulter centrifuge (FX6100 rotor, 20 °C) during 30 min at 1792 g (4000 rpm). The olive-colour supernatant was carefully decanted from the black sediment and collected in a conical centrifuge tube for further experiments.

2.4.2. Oligonucleotides preparation

Stock solutions of Tetra-A-ORF-FAM were reconstituted at a final concentration of 100 μM with sterilized purified Milli-Q water. Stock solutions of the thiolated oligonucleotides (Tetra-B, Tetra-C and Tetra-D) were prepared following the protocol for thiol-modified oligonucleotide reduction using 1,4-Dithiothreitol (DTT) and a NAP-10 column of Sephadex G-25. Stock solutions of the non-thiolated oligonucleotides (ORF-WT, SC1, and ORF-NC) were reconstituted at a final concentration of 100 μM with PBS (10 mM phosphate buffer 0.4 M NaCl pH 7.0). All stock solutions were stored at −20 °C in aliquots of a few microliters.

2.4.3. Tetrahedral DNA nanostructures synthesis

The four oligonucleotides (Tetra-A/Tetra-A-ORF/Tetra-A-ORF-FAM, Tetra-B, Tetra-C and Tetra-D; listed in Table S1) were mixed in equimolar quantities in TM buffer (20 mM Tris 50 mM MgCl2 pH 8.0). Then, the mixture was subjected in a thermocycler to a treatment based on three different stages divided into steps of 2 min each. Specifically, the first stage consists of 2 different steps at 95 °C and 51 °C; the second one of 4 steps at 46.1 °C, 43.6 °C, 41.2 °C and 38.8 °C; and the last one of 2 steps of 30 °C and 4 °C.

2.4.4. Bioconjugate (2D-MoS_2-TDN) preparation

Firstly, an aqueous solution of molybdenum disulphide was prepared. For this purpose, 2D-MoS_2 suspension was filtered using a 3 KDa filter and centrifugation (5 min, 10000 rpm) followed by a subsequent resuspension of the pellet in water. Next, the aqueous suspension of molybdenum disulphide was incubated overnight at room temperature with the previously synthesized tetrahedral DNA nanostructures (TDNs). After that, a washing step was carried out to remove non-absorbed molecules consisting of a second centrifugation (3 min, 10000 rpm), separating the nanostructured bioconjugate (2D-MoS_2-TDN) from the TDNs that have not been immobilized over the 2D-MoS_2 surface.

2.4.5. Detection of SARS-CoV-2 ORF1ab gene

100 μL of bioconjugate (2D-MoS_2-TDN) were challenged with 10.0 μL of the analyte in different concentrations (ORF-WT) and incubated in humid chamber at 37 °C for 1 h. The prepared solution was let to cool down to room temperature. Afterwards, a separation step was carried out based on a centrifugation (3 min, 7000 rpm) and resuspending in a final volume of 110 μL. After that, the excitation spectrum of the mixture was measured in the range 200–800 nm. Subsequently, the obtained excitation wavelength for the fluorophore was chosen (487 nm) and the emission spectrum was carried out, measuring fluorescence intensity through peak height.

2.4.6. Detection of SARS-CoV-2 in nasopharyngeal samples

100 μL of bioconjugate (2D-MoS_2-TDN) were challenged with 5.00 μL of the nasopharyngeal sample and incubated in humid chamber at 37 °C for 1 h. The prepared solution was let to cool down to room temperature. After that, the separation step and the emission spectrum were carried out under the same conditions of the above described.

3. Results and discussions

The first step to the development of the bioassay for rapid and easy virus detection was the preparation of the bioconjugate between the TDN and 2D-MoS_2.

3.1. Tetrahedral DNA nanostructure synthesis and characterization

The TDN was prepared by using three thiolated DNA 55-base long oligonucleotides (Tetra-B, Tetra-C, and Tetra-D) and a fourth 80-nucleotide strand (Tetra-A-ORF-FAM) that contains the DNA capture probe complementary to a specific SARS-CoV-2 gene region coding for the ORF1ab gene at its 5′ end modified with the fluorophore FAM. According to this design of the TDN, each oligonucleotide forms one of the 4 faces of the tetrahedron (Figure S1A). Each of them has a fragment of 17 base pairs complementary to each of the other three oligonucleotides. The complementary zones between them are indicated with the same color in Figure S1A and Table S1. The TDN has the ORF1ab capture probe labelled with FAM at one vertex (TDN-ORF), exposed to the solution and ready to hybridize with the target DNA, and three thiol groups at the basal vertices to be anchored to the 2D-MoS_2.

There are some procedures for TDN synthesis reported in the literature [22,29–32] that can give rise random structures. In this sense, we designed an improved synthesis method based on a slow and controlled temperature drop in several steps. We considered the melting temperature (Tm) of each of the complementary fragments that must hybridize with each other to obtain the desired structure, avoiding the formation of other undesired ones.

The Tm of each fragment used in the synthesis of TDN was calculated by the expression $Tm = 64.9 + 41\cdot(G + C\text{-}16.4)/L$ [33], where G and C are the number of guanine and cytosine bases, respectively, in the DNA sequence and L is the total number of bases (17 bases). Considering the resulting Tm, the procedure of TDN synthesis described in material and methods section was proposed.

To corroborate the efficacy of the proposed synthesis method, we characterized the resulting structures by electrophoretic analysis, cryogenic electron microscopy (cryo-EM) and optical microscopy (bright field and fluorescence).

Bright-field and fluorescence images of the of TDN-ORF-FAM immobilized on gold screen-printed electrodes are depicted in Figure S1C and D. As can be seen, the fluorescence corresponding to the FAM molecule attached to the TDN is observed (Figure S1D), confirming their successful synthesis, and anchoring on the gold surface.

Figure S1E shows the obtained gel electrophoresis. As it can be seen,

TDN-ORF (lane 5) moved more slowly than either each single-stranded DNA oligonucleotide (Tetra-A-ORF, Tetra-B, Tetra-C and Tetra-D, respectively, in lanes 1 to 4) or any trimer combination lacking one strand (TDN-ORF without Tetra-A-ORF, Tetra-B, Tetra-C or Tetra-D, respectively, in lanes 6 to 9). These results point out a successful synthesis of the TDN-ORF [26] and agree well with the cryo-EM images of TDN (Figure S1B).

Once the nanostructure is built, one vertex contains the capture probe available for the biorecognition reaction, while the other three vertices are thiolated for 2D-MoS_2 surface modification.

3.2. Liquid phase exfoliation of 2D-MoS_2

Liquid phase exfoliation of 2D-MoS_2 nanosheets was carried out as described in detail in the experimental section and using bulk MoS_2 as the precursor [28]. This mixture was cooled down and sonicated, prior a centrifugation step. Finally, the supernatant was decanted from the pellet, and it was resuspended on 2-propanol and water (7:3).

3.3. Tetrahedral DNA bioconjugate (2D-MoS_2-TDN) preparation and characterization

Once TDNs are synthesized and 2D-MoS_2 is resuspended in water, both precursors are challenged. 2D-MoS_2 -TDN bioconjugate is formed through the thiol groups of the TDN that tend to eliminate or repair sulphur vacancies of the 2D-MoS_2 surface, resulting in the functionalization of the nanomaterial lattice (2D-MoS_2-TDN) [17] as can be seen in Fig. 1A.

The percentage of the TDN immobilized on the 2D-MoS_2 was calculated using 6-FAM labelled TDN-ORF (TDN-ORF-FAM) through the measurement of the DNA UV–Vis signal of the bioconjugate at 260 nm. By measuring the absorbance of TDN-ORF-FAM solutions of different concentrations, a molar absorptivity coefficient of 1.96 L (μmol cm)$^{-1}$ was obtained for the DNA nanostructure (see Figure S2). Once this value is obtained, the percentage of immobilized DNA was calculated by introducing the absorbance signal from the nanostructured bioconjugate (see Fig. 1B, red curve) on the obtained linear fitting. A TDN-ORF-FAM concentration of 0.373 μM was obtained and, since initial concentration of TDN-ORF-FAM is 0.400 μM, it can be estimated that around 93% of the TDNs modify the 2D-MoS_2 surface.

The different steps followed for the bioconjugate preparation were characterized through different techniques in order to obtain the information that allow to stablish the optimal conditions and, consequently, to obtain reproducible results. UV–Vis spectra of 2D-MoS_2 nanosheets (blue curve) and 2D-MoS_2-TDN suspensions (red curve) show (see Fig. 1B) the characteristic A and B peaks of 2D-MoS_2 suspensions in water at 623 and 684 nm, respectively, in both curves [34]. A clear difference based on two peaks is shown between the nanomaterial (blue curve) and the bioconjugate spectra (red curve). On the red curve, a distinguishing peak due to the fluorophore (FAM) and a significant peak ascribed to DNA [35] is observed at 491 and 260 nm, respectively. Fluorescence has also been used in order to characterize different steps of the bioconjugate preparation. As it is portraited in Fig. 1C, there is practically no fluorescent signal for 2D-MoS_2 (blue curve), since this nanomaterial does not have any fluorescent properties. Once the TDN carrying the fluorophore is immobilized on the 2D-MoS_2, although the fluorophore is over the sensing platform, it does not emit any fluorescent signal (black curve), indicating that MoS_2 has a fluoresce quenching effect. After the FAM labelled probe hybridizes with the analyte (a totally complementary sequence of the probe, ORF-WT), there is

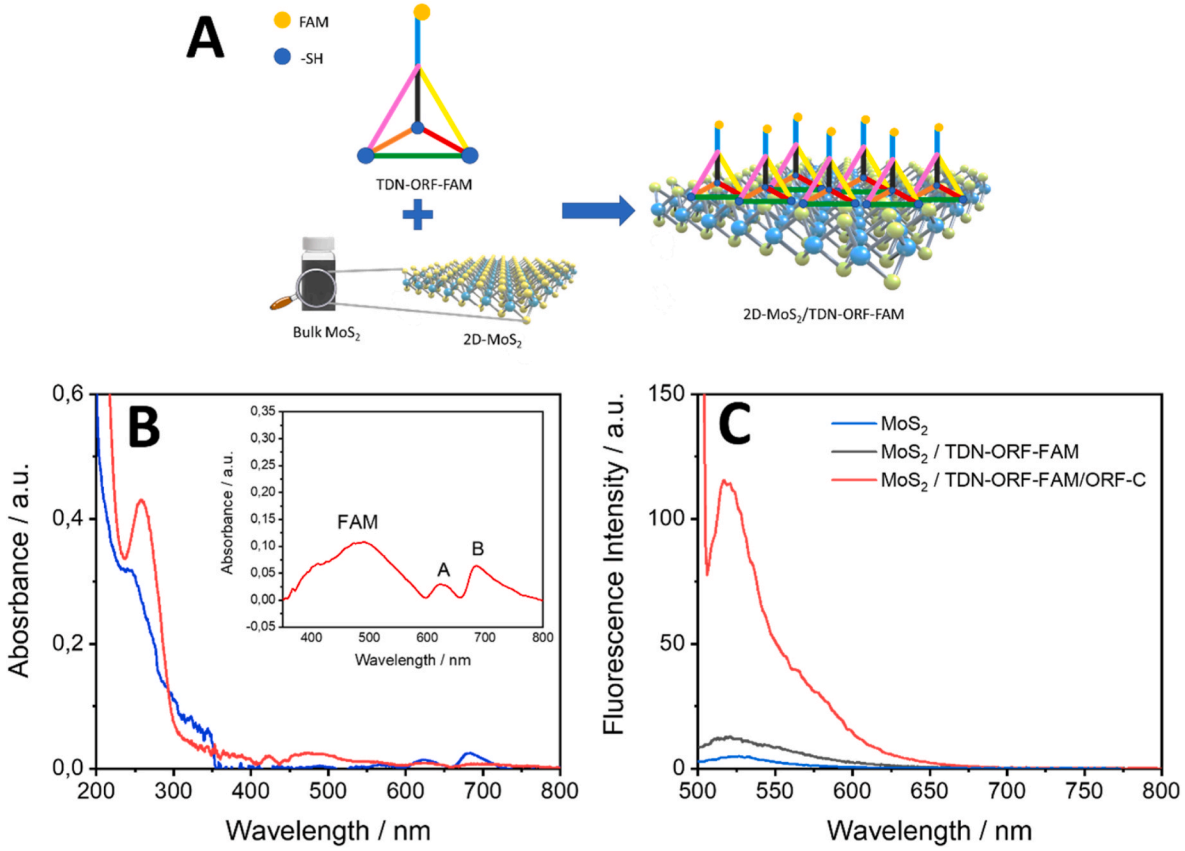


Fig. 1. (A) Scheme for bioconjugate (2D-MoS_2-TDN-ORF) development. (B) UV–Vis absorbance spectra of 2D-MoS_2 nanosheets (blue curve) and 2D-MoS_2-TDN (red curve). Inset: Amplified UV-absorbance spectra of 2D-MoS_2-TDN. (C) Fluorescence spectra of MoS_2 (blue curve); 2D-MoS_2-TDN (black curve) and 2D-MoS_2-TDN/ORF-WT (red curve) at an excitation wavelength of 487 nm.

a significant increase of the fluorescence signal (red curve). The fluorescent signal of FAM is recovered by the hybridization recognition reaction. Based on previously reported results [24,36], this fact is due to FAM fluorophore undergoing a fluorescence quenching by MoS_2 due to Van der Waals interactions between the nanomaterial and the fluorophore resulting in energy resonance transfer. This effect is also observed on dye-labelled single-stranded DNA [16]. When the target ORF-WT was added, hybridization is performed, forming the dsDNA containing FAM fluorophore with the emission maximum at 518 nm at excitation wavelength of 487 nm. The Van der Waals forces between the dsDNA formed after hybridization and MoS2 nanosheets are significantly weakened, which results in the recovery of the fluorescence intensity. These results not only demonstrate the bioconjugate formation but also are the base of the developed "signal off-on" fluorescence bioassay.

As well, Raman spectroscopy was carried out with the objective of characterizing the bioconjugate. As it is shown in Figure S3 in Supporting Information, 2D-MoS_2 spectra (black curve) show the characteristic bands for 2D-MoS_2, which corresponds to the 2H polytype structure of this material. These bands are found to be at 381 and 406 cm^{-1} that correspond to in-plane E_{12g} and out-of-plane A_{1g} (A and B, respectively) vibration modes of 2H MoS_2 [37]. On the TDN Raman spectra (red curve), signals for guanine (594 and 681 cm^{-1}), thymine (748 cm-1), adenine (1143 and 1342 cm^{-1}), cytosine (1183 cm^{-1}) and the DNA phosphate backbone (832, 954, 1008 and 1452 cm^{-1}) are found [38]. Finally, on the bioconjugate spectra (blue curve) previously mentioned signals for 2D-MoS_2 and TDNs are found, thus, the immobilization of the TDNs over the 2D-MoS_2 lattice is demonstrated.

The characterization of the bioconjugate was also performed by EDAX and Fluorescence microscopy. Fig. 2B show the EDAX spectra of MoS_2 flakes on gold where the presence of the peaks corresponding to the energies of Mo, S and Au can be observed. The spectra of the bioconjugate on gold (Fig. 2D) is similar to the previous one due to the fact that the energies of the peaks corresponding to P and Au are very close. Therefore, the peaks overlap, and those two elements cannot be distinguished. To probe the presence of P from the TDN, the bioconjugate was deposited on highly oriented pyrolytic graphite (HOPG) instead of gold. The absence of gold allows for the detection of the isolated peak that corresponds to the energy of P (Fig. 2E), indicating the presence of DNA. Fig. 4 shows the fluorescence optical microscopy images of gold and HOPG substrates modified with 2D-MoS_2 or 2D-MoS_2-TDN bioconjugate. Contrast can only be observed in the Fluorescence images, where the bioconjugate is present (See Figure S4D and F in Supporting Information) revealing the presence of TDN-ORF-FAM. As control experiments, EDAX spectra and Fluorescence microscopy images of the bare substrate (gold) were carried out (See Figure S5 in Supporting Information), in this case no fluorescence is observed.

Fig. 3 shows the AFM images and profile of the topography of 2D-MoS_2 on gold (A, C and E) and of 2D-MoS_2-TDN on gold (B, D and F). The gold topography image and profile is shown in Figure S3. On 14 selected areas of the Au/2D-MoS_2 and Au/2D-MoS_2-TDN we have performed a roughness analysis (See Figure S6 in Supporting Information). As can be

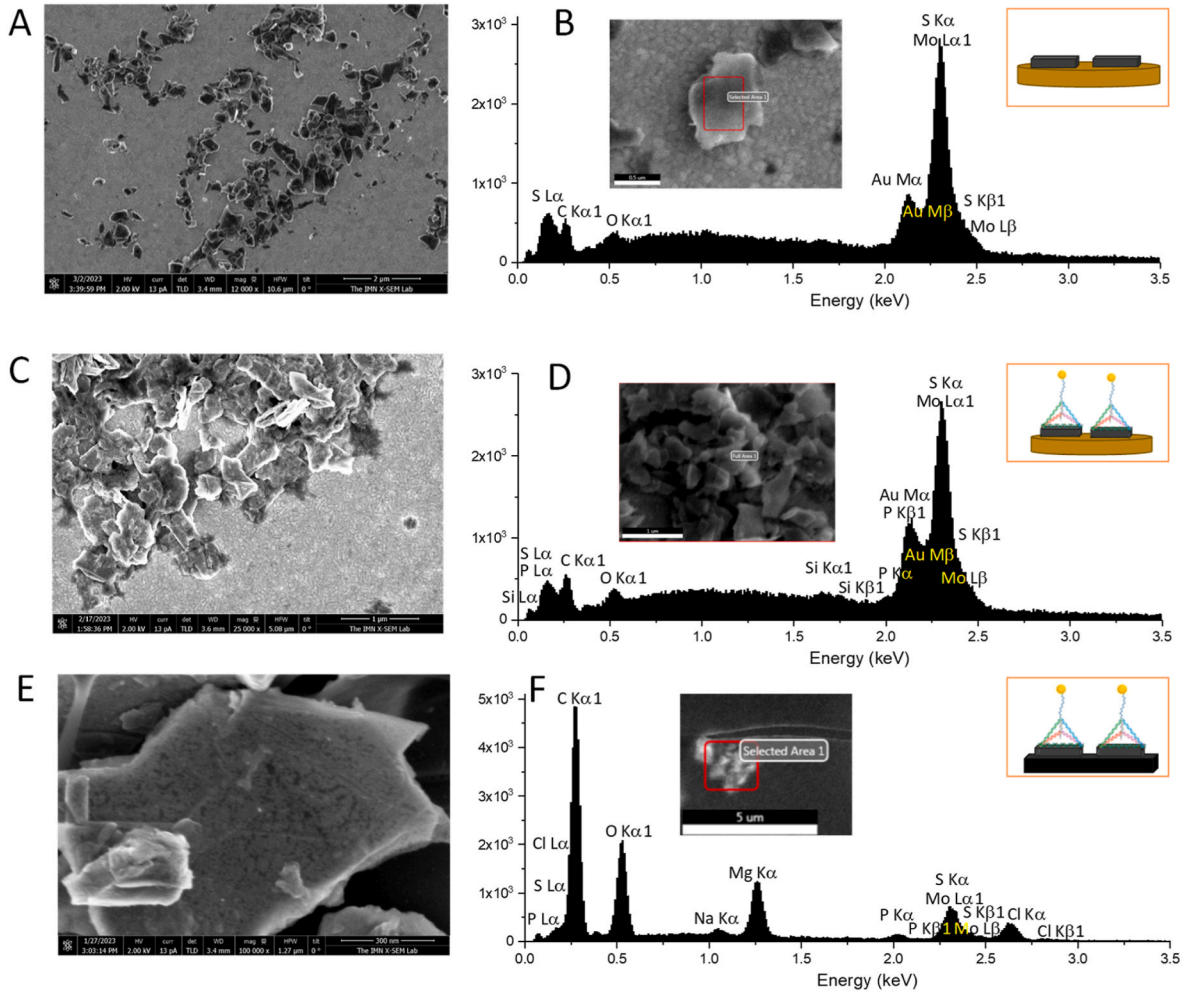


Fig. 2. SEM images (A, C, E) and EDX spectra (B, D, F) of the selected area of: (A, B) 2D-MoS_2 over gold substrate (Au/MoS_2) (C, D) 2D-MoS_2-TDN over gold substrate (Au/2D-MoS_2-TDN) and (E,F) 2D-MoS_2-TDN over highly oriented pyrolytic graphite (HOPG/2D-MoS_2-TDN). 5 kV, resolution: 128 eV.

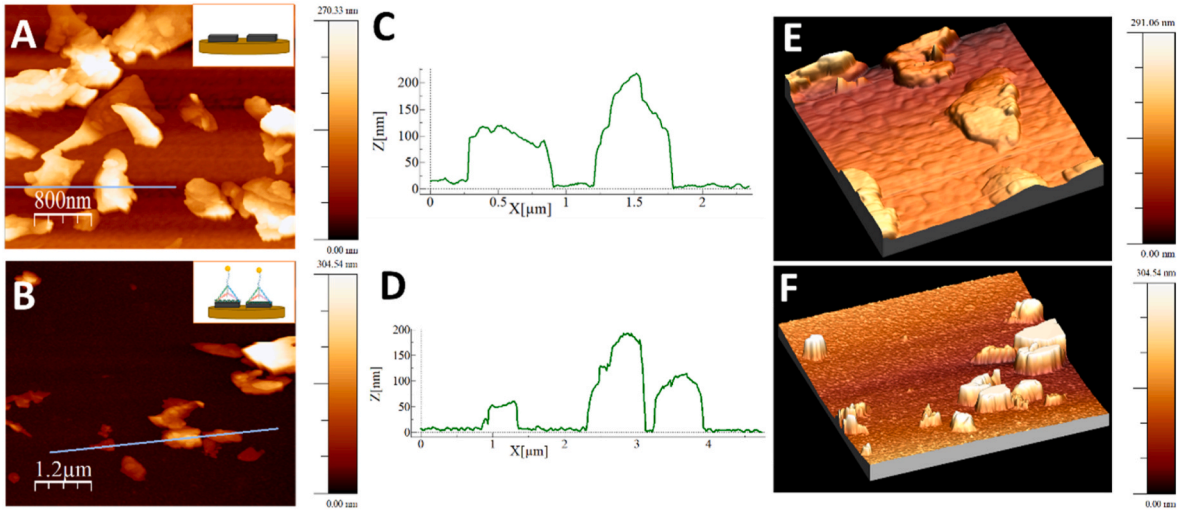


Fig. 3. AFM images of (A) Au/2D-MoS_2 and (B) Au/2D-MoS_2-TDN over gold; their respective profiles shown in the images (C from A and D from B) and their respective three-dimensional images (E from A and B from F).

observed, the RMS roughness is higher in the case of 2D-MoS_2-TDN. In particular, a mean value of roughness of 2,1 ± 0,9 and 3,0 ± 1,3 nm for the Au/2D-MoS_2 and Au/2D-MoS_2-TDN, respectively, were observed. This increase in roughness could be attributed to the modification of the 2D-MoS_2 with the TDNs.

3.4. Bioassay development

Once the bioconjugate was characterized, it was employed for the development of the bioassay for rapid virus detection, taking as case of study the detection of SARS-CoV-2 virus through the detection of a specific DNA sequence of the ORF1ab gene. The scheme of the proposed optical bioassay is depicted in Fig. 4A. Once the bioconjugate (2D-MoS_2-TDN) is obtained, it is then challenged with the complementary strand, the SARS-CoV-2 ORF1ab gene (ORF-WT). The biorecognition reaction is followed by the change of the fluorescence signal of the bioconjugate. As it can be seen in Fig. 4B there is a gradual fluorescence increase on increasing the concentration of ORF-WT in solution (100 fM, 250 fM, 375 fM, 500 fM, 625 fM, 750 fM, 875 fM and 1.00 pM).

2D-MoS_2 plays a key role in fluorescence quenching and recovery. The same assay was carried out without using 2D-MoS_2 and no significant difference in the fluorescence signal between the tetrahedral DNA nanostructure before and after being challenged with the sequence analyte was found.

Fig. 4C shows that the signal increase is linear with the ORF-WT concentration (If = 34.0 + 0.0730·[ORF-WT]; R = 0.9889). The values presented were obtained from the mean of three different measurements for every concentration, leaving a percentage coefficient of variation (CV) of 2% and a sensitivity of 0.0730 a.u. (fM^{-1}). The limit of detection (LOD) and quantification (LOQ) were calculated through $3{\cdot}S_b{\cdot}m$ and $10{\cdot}S_b{\cdot}m$ criteria, respectively, where S_b corresponds to the standard deviation of the blank signal (signal obtained incubating with saline phosphate buffer without the analyte) and m is the slope of the linear fitting. The blank signal was measured 10 times and a LOD and a LOQ of 19.7 fM and 65.6 fM respectively, were obtained. These values were experimentally proven. Reproducibility was estimated from the mean and the standard deviation of three different assays using three different bioconjugates prepared following the same protocol. The reproducibility is expressed in percentage of coefficient of variation (CV (%)) by using the errors obtained in the calibration plot. The range of CV (%) covered from 1.3 % (875 fM) to 4.2% (375 fM).

In addition, the selectivity of the bioassay was also evaluated. The fluorescent signal of three different samples containing the analyte (ORF-WT) in a concentration of 750 fM in the absence or presence of potential interfering sequences was measured. Among the possible interferees, two viral sequences were evaluated: SARS-CoV-1 (SC1) and Influenza A (ORF-NC) both at a concentration of 750 fM. As it is shown on Fig. 4D, the intensity of the fluorescent signal does not suffer a significant change in the absence or presence of a possible interferent. These results demonstrate that the developed bioassay is capable of detect a specific sequence of the SARS-CoV-2 genome, discerning between this analyte and possible interferents.

Finally, we wanted to go one step forward to assess the selectivity of the bioassay and we employed as analyte a ORF sequence carrying a mismatch. As it is portraited in Fig. 4E, there is a significant difference in the fluorescence intensity measured when with the analyte is the totally complementary sequence or one carrying a mismatch. When the bioconjugate is challenged with the mismatched strand a lower signal is obtained, probably due to partial hybridization with the capture probe. Therefore, the designed bioassay can differentiate between the ORF1ab and its mutations, opening the door for the development of new biosensing platforms that can distinguish between different COVID-19 variants.

In order to study the real utility of the developed bioassay for rapid virus detection, it was applied to nasopharyngeal samples from COVID-19 infected patients. The samples were provided by Hospital Ramón y Cajal and were also analyzed using RT-qPCR. Three samples were used: one corresponding to a non-infected patient and the other two to patients with different viral loads (P1, 29 Cts and P2, 15 Cts, these values were obtained in the Hospital through RT-qPCR). As it can be observed in Fig. 5, the developed bioassay is able to distinguish between the two nasopharyngeal samples with viral loads of 29 and 15 Cts, respectively, and from a non-infected patient sample. Therefore, it can be concluded that the developed bioassay can be employed to detect a SARS-CoV-2 DNA sequence from human nasopharyngeal samples in a rapid and easy way compared to the time consuming and more expensive gold standard method.

Lastly, the stability of the bioconjugate was evaluated by measuring the bioassay response for 30 days when it was stored at 4 °C. The results showed that the initial signal was kept at a 90% after 30 days (see Figure S7 in Supporting Information).

The developed bioassay has a wide range of applicability since it can be applied to the detection of any pathogen by changing the probe corresponding to the target sequence. Thus, a novel, hands-on strategy for rapid pathogen detection has proposed and has a high potential application value in the early diagnosis of infections causes by virus or

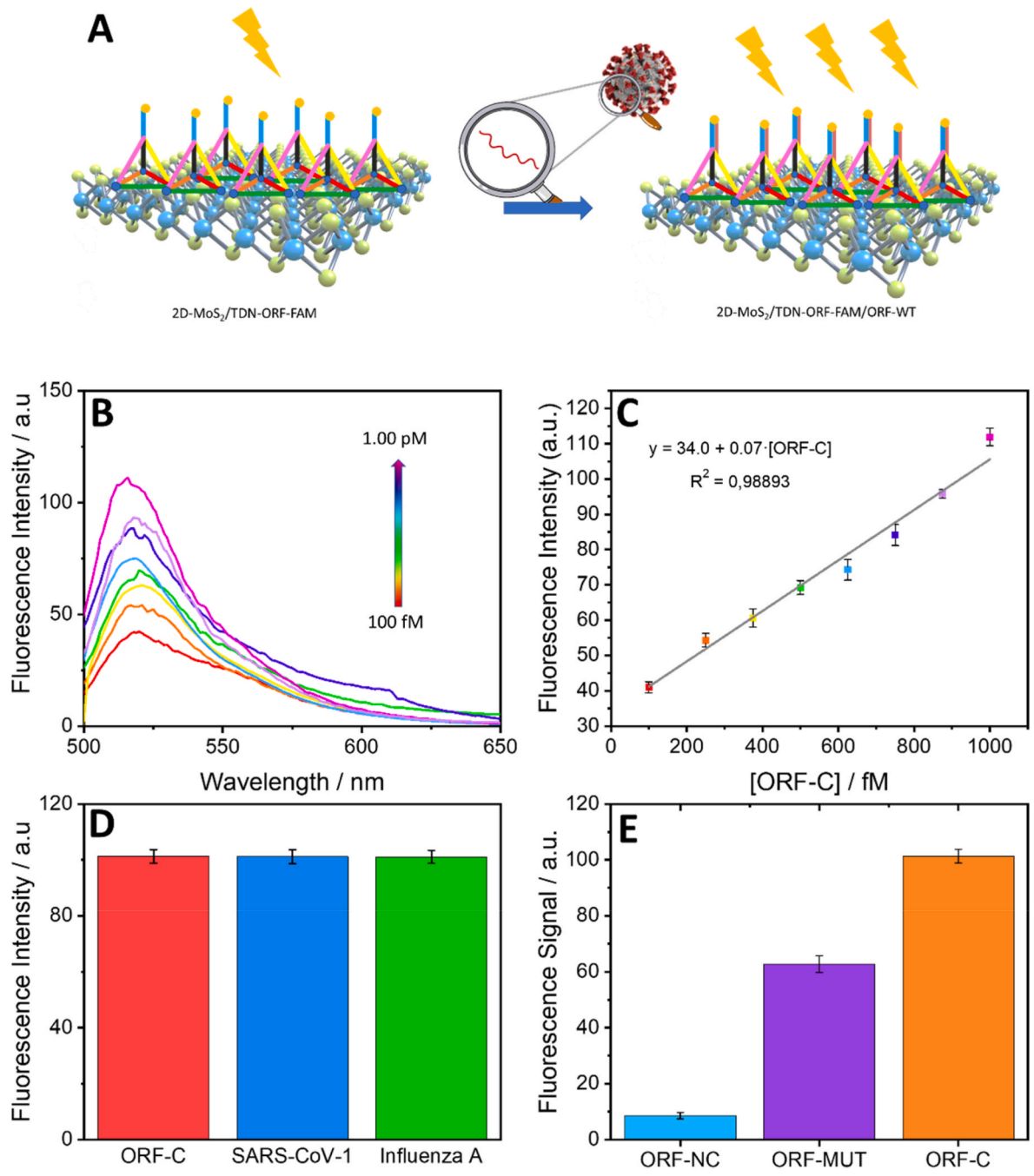


Fig. 4. (A) Scheme for TDN and MoS_2-based fluorescent bioassay for SARS-CoV-2 ORF1ab gene detection. (B) Fluorescence spectra of the bioconjugate after hybridization with increasing amounts of ORF-WT (100 fM (red curve), 250 fM (orange curve), 375 fM (yellow curve), 500 fM (green curve), 625 fM (blue curve), 750 fM (dark blue curve), 875 fM (purple curve), 1.00 pM (pink curve)) using λ_{exc} = 487 nm. (C) Obtained calibration plot. (D) Fluorescence intensity obtained in the absence and presence of potential interferents (ORF-WT 750 fM (red bar); ORF-WT + SC1 750 fM (blue bar) and ORF-WT + ORF-NC 750 fM (green bar)). (E) Fluorescence intensity obtained of the bioconjugate after challenged with ORF-MUT (750 fM, purple bar) and ORF-WT (750 fM, orange bar). Blank signal with PBS (blue bar).

bacteria.

4. Conclusions

A new fluorescent bioassay based on the use of a 2D-MoS_2/TDN bioconjugate has been developed and proposed as an efficient alternative to detect pathogens, specifically SARS-CoV-2. 2D-MoS_2 allows the anchoring of thiol groups through sulphur vacancies, thus, the designed TDN can be immobilized over the nanomaterial lattice. Through this process some advantages are obtained such as signal amplification. This nanostructured bioconjugate can detect a specific SARS-CoV-2 DNA sequence, ORF1ab, with detection and quantification limits of 19.7 and 65.6 fM, respectively. Overmore, the bioconjugate is capable of detecting ORF1ab sequence in the presence of potential interferents. The bioconjugate shows great stability when stored at 4 °C and its applicability has been proved by detecting SARS-CoV-2 in nasopharyngeal samples from COVID-19 infected patients, not being necessary any amplification process. Furthermore, the developed bioassay has a wide range of applicability since it can be applied to the detection of any pathogen.

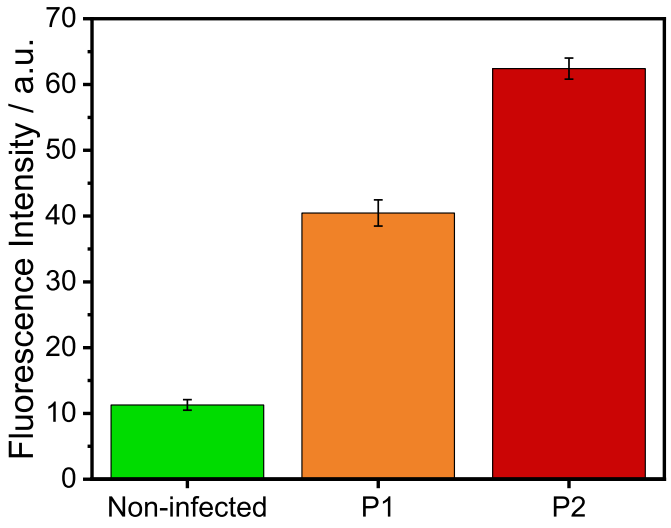


Fig. 5. Bioassay response to human nasopharyngeal samples of non-infected SARS-CoV-2 patient (green bar) and infected patients (P1 (29 Cts, orange bar) and P2 (15 Cts, red bar)).

CRediT authorship contribution statement

Daniel García- Fernández: Data curation, Methodology, Writing - original draft. **Laura Gutiérrez- Gálvez:** Data curation, Formal analysis. **Manuel Vázquez Sulleiro:** Data curation, Investigation, Methodology. **Marina Garrido:** Data curation, Methodology. **David López-Diego:** Data curation, Investigation. **Mónica Luna:** Conceptualization, Data curation, Formal analysis, Funding acquisition, Writing - review & editing. **Emilio M. Pérez:** Conceptualization, Funding acquisition, Investigation, Writing - review & editing. **Tania García-Mendiola:** Conceptualization, Funding acquisition, Project administration, Writing - original draft, Writing - review & editing. **Encarnación Lorenzo:** Conceptualization, Funding acquisition, Investigation, Writing - original draft, Writing - review & editing.

Declaration of competing interest

The authors declare that they have no known competing financial interests or personal relationships that could have appeared to influence the work reported in this paper.

Data availability

Data will be made available on request.

Acknowledgements

This work has been financially supported by the Spanish Ministry of Economy and Competitiveness ((PID2020-116728RB-I00, CTQ2015-71955-REDT (ELECTROBIONET)) and Community of Madrid (REACT-UE NANOCOV-CM, TRANSNANOAVANSENS, S2018/NMT-4349). Laura Gutiérrez-Gálvez was supported by a Formación del Profesorado Universitario (FPU) grant from the Spanish Ministry of Universities (FPU19/06309). Daniel García-Fernández was supported by a Programa Investigo grant from Autonomous Community of Madrid in the framework of the Plan de Recuperación, Transformación y Resiliencia financed by the European Union – NextGenerationEU (09-PIN1-00013.4/2022-Puesto 83). The authors acknowledge the support of the European Union (EU) and Horizon 2020 through Instruct Proposal PID: 21859, and the CRIOMECORR project (ESFRI-2019-01-CSIC-16) to the cryoEM CNB-CSIC facility. We also acknowledge María U. González help with Fluorescence Microscopy and the service from the MiNa Laboratory at IMN, and funding from CM (project S2018/NMT-4291 TEC2SPACE), MINECO (project CSIC13-4E-1794) and EU (FEDER, FSE). IMDEA Nanociencia acknowledges support from the 'Severo Ochoa' Programme for Centres of Excellence in R&D (MINECO, CEX2020-001039-S).

Authors acknowledges Alvaro Somoza, Milagros Castellanos from IMDEA Nanociencia and IRYCIS for the nasopharyngeal samples from COVID-19 infected patients supplied.

Appendix A. Supplementary data

Supplementary data to this article can be found online at https://doi.org/10.1016/j.talanta.2023.125497.

References

[1] C.F. Meares, Bioconjugate chemistry, in: Reference Module in Chemistry, Molecular Sciences and Chemical Engineering, Elsevier, 2014, https://doi.org/10.1016/b978-0-12-409547-2.11087-x.
[2] Y. Zheng, R. Xu, S. Chen, W. Tai, In vivo therapeutic effects of small molecule-drug conjugates enhanced by Fc grafting, Biomaterials (2022) 290, https://doi.org/10.1016/j.biomaterials.2022.121820.
[3] O.C. Didamson, R. Chandran, H. Abrahamse, A gold nanoparticle bioconjugate delivery system for active targeted photodynamic therapy of cancer and cancer stem cells, Cancers (Basel) 14 (2022), https://doi.org/10.3390/cancers14194558.
[4] X. Shi, P. Xu, C. Cao, Z. Cheng, J. Tian, Z. Hu, PET/NIR-II fluorescence imaging and image-guided surgery of glioblastoma using a folate receptor α-targeted dual-modal nanoprobe, Eur. J. Nucl. Med. Mol. Imag. 49 (2022) 4325–4337, https://doi.org/10.1007/s00259-022-05890-x.
[5] P.P. Pednekar, K.R. Jadhav, V.J. Kadam, Aptamer-dendrimer bioconjugate: a nanotool for therapeutics, diagnosis, and imaging, Expet Opin. Drug Deliv. 9 (2012) 1273–1288, https://doi.org/10.1517/17425247.2012.716421.
[6] W. Tai, Current aspects of siRNA bioconjugate for in vitro and in vivo delivery, Molecules 24 (2019), https://doi.org/10.3390/molecules24122211.
[7] R.G. Mahmudunnabi, M. Umer, K.D. Seo, D.S. Park, J.H. Chung, M.J.A. Shiddiky, Y.B. Shim, Exosomal microRNAs array sensor with a bioconjugate composed of p53 protein and hydrazine for the specific lung cancer detection, Biosens. Bioelectron. 207 (2022), https://doi.org/10.1016/j.bios.2022.114149.
[8] Y. Wang, F. Wang, Z. Han, K. Huang, X. Wang, Z. Liu, S. Wang, Y. Lu, Construction of sandwiched self-powered biosensor based on smart nanostructure and capacitor: toward multiple signal amplification for thrombin detection, Sensor. Actuator. B Chem. 304 (2020), https://doi.org/10.1016/j.snb.2019.127418.
[9] S. Kumar De, S. Ray, Y. Rawat, S. Mondal, A. Nandy, P. Verma, A. Roy, P. Sadhukhan, C. Das, S. Bhattacharyya, D. Senapati, Porous Au-seeded Ag nanorod networks conjugated with DNA aptamers for impedimetric sensing of DENV-2, Sensor. Actuator. B Chem. 348 (2021), https://doi.org/10.1016/j.snb.2021.130709.
[10] M. Mediavilla, M. Revenga-Parra, C. Gutiérrez-Sánchez, L. Hernández-Apaolaza, F. Pariente, E. Lorenzo, Fluorescent enzymatic assay for direct total polyphenol determination in food-related samples, Talanta 247 (2022), https://doi.org/10.1016/j.talanta.2022.123576.
[11] M.A. Ríos-Corripio, L.S. Arcila-Lozano, B.E. Garcia-Perez, M.E. Jaramillo-Flores, A. D. Hernández-Pérez, A. Carlos-Martínez, M. Rosales-Perez, M. Rojas-López, Fluorescent gold nanoparticle-based bioconjugate for the detection of Salmonella, Anal. Lett. 49 (2016) 1862–1873, https://doi.org/10.1080/00032719.2015.1128944.
[12] N. Hildebrandt, O. Tagit, Colloidal nanoparticles for signal enhancement in optical diagnostic assays, J. Nanosci. Nanotechnol. 18 (2018) 6671–6679, https://doi.org/10.1166/jnn.2018.15748.
[13] Z. Sun, J. Li, Y. Yang, Y. Tong, H. Li, C. Wang, L. Du, Y. Jiang, Ratiometric fluorescent biosensor based on self-assembled fluorescent gold nanoparticles and duplex-specific nuclease-assisted signal amplification for sensitive detection of exosomal miRNA, Bioconjugate Chem. 33 (2022) 1698–1706, https://doi.org/10.1021/acs.bioconjchem.2c00309.
[14] Y. Dong, W. Hu, M. Qian, Y. Wang, DNA aptamer-based fluorescence biosensor, Dianzi Yu Xinxi Xuebao/J. Electr. Inform. Technol. 42 (2020) 1374–1382, https://doi.org/10.11999/JEIT190860.
[15] W. Wang, W. Zhai, Y. Chen, Q. He, H. Zhang, Two-dimensional material-based virus detection, Sci. China Chem. 65 (2022) 497–513, https://doi.org/10.1007/s11426-021-1150-7.
[16] Y. Zhang, B. Zheng, C. Zhu, X. Zhang, C. Tan, H. Li, B. Chen, J. Yang, J. Chen, Y. Huang, L. Wang, H. Zhang, Single-layer transition metal dichalcogenide nanosheet-based nanosensors for rapid, sensitive, and multiplexed detection of DNA, Adv. Mater. 27 (2015) 935–939, https://doi.org/10.1002/adma.201404568.
[17] S. Catalán-Gómez, M. Briones, S. Cortijo-Campos, T. García-Mendiola, A. de Andrés, S. Garg, P. Kung, E. Lorenzo, J.L. Pau, A. Redondo-Cubero, Breast cancer biomarker detection through the photoluminescence of epitaxial monolayer MoS2 flakes, Sci. Rep. 10 (2020), https://doi.org/10.1038/s41598-020-73029-9.
[18] P.W.K. Rothemund, Folding DNA to create nanoscale shapes and patterns, Nature 440 (2006) 297–302, https://doi.org/10.1038/nature04586.
[19] P.L. Xavier, A.R. Chandrasekaran, DNA-Based Construction at the Nanoscale: Emerging Trends and Applications, 2018.

[20] L. Qian, E. Winfree, Scaling up digital circuit computation with DNA strand displacement cascades, Science (2011) 1196–1201, https://doi.org/10.1126/science.1200520 (1979). 332.
[21] H. Chai, Y. Tang, P. Miao, Tetrahedral DNA supported walking nanomachine for ultrasensitive miRNA detection in cancer cells and serums, Anal. Chem. 94 (2022) 9975–9980, https://doi.org/10.1021/acs.analchem.2c02288.
[22] Z. Ge, M. Lin, P. Wang, H. Pei, J. Yan, J. Shi, Q. Huang, D. He, C. Fan, X. Zuo, Hybridization chain reaction amplification of microRNA detection with a tetrahedral DNA nanostructure-based electrochemical biosensor, Anal. Chem. 86 (2014) 2124–2130, https://doi.org/10.1021/ac4037262.
[23] M. Zhao, R. Wang, K. Yang, Y. Jiang, Y. Peng, Y. Li, Z. Zhang, J. Ding, S. Shi, Nucleic acid nanoassembly-enhanced RNA therapeutics and diagnosis, Acta Pharm. Sin. B 13 (2023) 916–941, https://doi.org/10.1016/j.apsb.2022.10.019.
[24] A. Podder, H.J. Lee, B.H. Kim, Fluorescent nucleic acid systems for biosensor, Bull. Chem. Soc. Jpn. 94 (2021) 1010–1035, https://doi.org/10.1246/BCSJ.20200351.
[25] X. Zhao, R. Tapec-Dytioco, W. Tan, Ultrasensitive DNA detection using highly fluorescent bioconjugated nanoparticles, J. Am. Chem. Soc. 125 (2003) 11474–11475, https://doi.org/10.1021/ja0358854.
[26] H. Pei, N. Lu, Y. Wen, S. Song, Y. Liu, H. Yan, C. Fan, A DNA nanostructure-based biomolecular probe carrier platform for electrochemical biosensing, Adv. Mater. 22 (2010) 4754–4758, https://doi.org/10.1002/adma.201002767.
[27] I. Horcas, R. Fernández, J.M. Gómez-Rodríguez, J. Colchero, J. Gómez-Herrero, A. M. Baro, WSXM, A software for scanning probe microscopy and a tool for nanotechnology, Rev. Sci. Instrum. 78 (2007), https://doi.org/10.1063/1.2432410.
[28] E. Giovanelli, A. Castellanos-Gomez, E.M. Pérez, Surfactant-free polar-to-nonpolar phase transfer of exfoliated MoS2 two-dimensional colloids, Chempluschem 82 (2017) 732–741, https://doi.org/10.1002/cplu.201700038.
[29] Z. Li, B. Zhao, D. Wang, Y. Wen, G. Liu, H. Dong, S. Song, C. Fan, DNA nanostructure-based universal microarray platform for high-efficiency multiplex bioanalysis in biofluids, ACS Appl. Mater. Interfaces 6 (2014) 17944–17953, https://doi.org/10.1021/am5047735.
[30] N. Mitchell, R. Schlapak, M. Kastner, D. Armitage, W. Chrzanowski, J. Riener, P. Hinterdorfer, A. Ebner, S. Howorka, A DNA nanostructure for the functional assembly of chemical groups with tunable stoichiometry and defined nanoscale geometry, Angew. Chem. Int. Ed. 48 (2009) 525–527, https://doi.org/10.1002/anie.200804264.
[31] Y. Wen, H. Pei, Y. Wan, Y. Su, Q. Huang, S. Song, C. Fan, DNA nanostructure-decorated surfaces for enhanced aptamer-target binding and electrochemical cocaine sensors, Anal. Chem. 83 (2011) 7418–7423, https://doi.org/10.1021/ac201491p.
[32] Y. Wen, H. Pei, Y. Shen, J. Xi, M. Lin, N. Lu, X. Shen, J. Li, C. Fan, DNA Nanostructure-based Interfacial engineering for PCR-free ultrasensitive electrochemical analysis of microRNA, Sci. Rep. 2 (2012), https://doi.org/10.1038/srep00867.
[33] R. Kalendar, D. Lee, A.H. Schulman, FastPCR software for PCR primer and probe design and repeat search Complexity of repeat sequences in differential genomes of plant/animal infecting viruses View project PCR and qPCR assays development View project. https://www.researchgate.net/publication/284652273, 2009.
[34] V. Forsberg, R. Zhang, J. Bäckström, C. Dahlström, B. Andres, M. Norgren, M. Andersson, M. Hummelgård, H. Olin, Exfoliated MoS2 in water without additives, PLoS One 11 (2016), https://doi.org/10.1371/journal.pone.0154522.
[35] M. Marieeswaran, P. Panneerselvam, Fluorescent polyaniline nanoclips (PANCs): a highly sensitive and selective chemical sensor for the detection of Hg (II) ions in aqueous media, ChemistrySelect 5 (2020) 4481–4487, https://doi.org/10.1002/slct.202000545.
[36] J. Wei, S. He, Y. Mao, L. Wu, X. Liu, C.Y. Effah, H. Guo, Y. Wu, A simple “signal off–on” fluorescence nanoplatform for the label-free quantification of exosome-derived microRNA-21 in lung cancer plasma, Microchim. Acta 188 (2021), https://doi.org/10.1007/s00604-021-05051-1.
[37] R. Luo, W.W. Xu, Y. Zhang, Z. Wang, X. Wang, Y. Gao, P. Liu, M. Chen, Van der Waals interfacial reconstruction in monolayer transition-metal dichalcogenides and gold heterojunctions, Nat. Commun. 11 (2020), https://doi.org/10.1038/s41467-020-14753-8.
[38] B. Prescott, W. Steinmetz, G.J. Thomas, Characterization of DNA Structures by Laser Raman Spectroscopy*, n.d.